Clean Technology for Resource, Energy and Environment

jcleantree.com

Review Article

Algae-derived Electrocatalysts for Energy Applications: Synthesis, Performance and Prospects

Yashu Guo[1,2], Lei Ding[3], Hongyu Liu[1,2], Ning-Hao Wang[4] and Dongle Cheng[5,*]

[1]*Key Laboratory of Groundwater Resources and Environment (Jilin University), Ministry of Education, Jilin University, Changchun 130021, Jilin, China*

[2]*Jilin Provincial Key Laboratory of Water Resources and Environment, Jilin University, Changchun 130021, Jilin, China*

[3]*Centre for Atomaterials and Nanomanufacturing, School of Science, RMIT University, Melbourne, Victoria, Australia.*

[4]*Department of Chemistry, Northeastern University, Shenyang, China*

[5]*College of Safety and Environmental Engineering, Shandong University of Science and Technology, Qingdao, Shandong 266590, China; Email: donglelecheng@gmail.com*

Cite This: https://doi.org/xxxxx-xxxxx-xxxxx

Read Online

ABSTRACT: In recent years, the overgrowth of certain algae species has posed a potential risk to the aquatic environment and ecological balance. However, algal biomass can serve as an ideal precursor for sustainable catalysts due to its rapid growth, widespread distribution, renewable nature, and low cost. The rational utilization of waste algae represents a dual innovative strategy for environmental remediation and energy conversion. This review systematically summarizes recent advances in algae biomass-derived electrocatalysts, beginning with an overview of common synthesis methods, including pyrolysis and protein-assisted sol–gel processes, and emphasizing their structural and functional merits. Benefiting from the intrinsic heteroatoms and natural cellular architectures of algal biomass, algae-derived carbon materials exhibit high specific surface areas, which contribute to structural optimization and enhanced electronic properties. This review provides guidance for future research on bio-derived catalysts.

Keywords: Algal biomass; Bio-derived electrocatalysts; Energy conversion; Carbon materials; Sustainable catalysis.

1. INTRODUCTION

The global energy crisis and environmental challenges have become increasingly severe [1, 2]. Electrochemical reactions such as the oxygen reduction reaction (ORR), oxygen evolution reaction (OER), hydrogen evolution reaction (HER), and carbon dioxide reduction reaction (CO_2RR) are essential for environmental remediation and clean energy conversion [3, 4]. However, these multi-electron transfer processes generally suffer from high reaction energy barriers and sluggish kinetics [5]. Therefore, searching for efficient electrocatalysts to enhance reaction efficiency has become critically important [6]. Although noble metals and their alloys (e.g., Pt, Ir, Ru) have been developed as benchmark catalysts, their high cost and limited availability restrict large-scale applications [7]. Consequently, the development of low-cost, sustainable, and highly efficient catalysts have emerged as a major research focus in recent years.

In recent years, biomass-derived carbon materials have been widely investigated as promising candidates to address the aforementioned challenges [8, 9]. Among various biomass resources, algae have attracted particular attention due to their unique advantages,

Received: September 05, 2025
Accepted: October 08, 2025
Published: December 16, 2025

including rapid growth, high nutrient uptake efficiency, and broad distribution in aquatic systems [10, 11]. As a natural and abundant biomass, algae are easily accessible and cost-effective. However, the excessive proliferation of certain species, such as harmful algal blooms (HABs), can lead to oxygen depletion, water quality deterioration, and ecological imbalance [12]. Rational utilization of waste algae not only mitigates these negative impacts on aquatic ecosystems but also provides a renewable feedstock for catalyst development [13].

Algae possess strong nutrient absorption capacity and are inherently rich in carbohydrates, proteins, and lipids, along with heteroatoms such as nitrogen, silicon, and sulfur [14, 15]. These intrinsic biomolecular components can undergo in situ heteroatom doping and the construction of porous carbon frameworks through pyrolysis treatment [16]. In addition, the sol–gel method is frequently employed, wherein algae-derived biomass, after processing, is often combined with natural polymers such as agar and gelatin, serving as polymeric agents or templates for the synthesis of nanomaterials with controlled morphology, particle size, and composition [17, 18]. Such strategies significantly enhance the structural tunability and electron transfer capability of Algae-derived electrocatalysts, thereby reducing the energy barriers of multi-electron transfer reactions and accelerating the reaction kinetics [19].

This review systematically summarizes the recent advances in algae biomass-derived electrocatalysts. The primary focus is placed on their synthesis strategies, including pyrolysis treatment and sol–gel methods, together with representative case studies such as Sargassum spp. (SP), Microalgae (MA), Red Algae (RA), Seaweed (SW), Chlorella (CA), and harmful algal blooms (HABs). Their applications in ORR, OER, HER, and CO_2RR are discussed, with an emphasis on the correlation between the structural features of processed algal biomass and the resulting catalytic performance. Finally, the review provides perspectives on the rational utilization of algal biomass and waste harmful algae, offering new insights into the design of high-performance electrocatalysts from bio-derived carbons.

2. SYNTHESIS OF ALGAE-DERIVED ELECTROCATALYST

2.1. Pyrolysis Methods

Pyrolysis is the most commonly employed strategy for converting biomass into carbon-based electrocatalysts [20]. Pyrolysis typically involves thermal decomposition under an inert atmosphere (N_2 or Ar) at temperatures ranging from 400 to 1000°C [21, 22]. In addition, a general approach to optimizing porosity and structural features is chemical activation by introducing activating agents during pyrolysis. Commonly used activators include KOH, K_2CO_3, and $ZnCl_2$ [23]. These inherent heteroatoms significantly influence the electronic behavior of carbon structures. They promote the formation of pyridinic N/S-C active sites, which improve charge transport and alter how essential intermediates adsorb on the surface.

Algal biomass is characterized by its rapid growth rate and high nutrient uptake capacity, and is intrinsically rich in carbohydrates, proteins, and lipids. Moreover, the presence of heteroatoms such as nitrogen, sulfur, and silicon, together with its naturally porous structure, further endows algae with unique advantages as a precursor for carbon-based electrocatalysts [24]. The intrinsic heteroatoms (e.g., N, S, Si) and porous structures of algal biomass enable in situ self-doping during pyrolysis, leading to the formation of carbon materials with tunable morphologies and controlled heteroatom incorporation [25]. The enhanced catalytic activity was primarily attribute to the Ni active sites, which improved the gasification efficiency (GE) to 60.5%, thereby boosting the overall HER performance [26]. The improved HER behavior of Ni-modified algal carbon reflects a clear structural influence on catalytic function. Metal–carbon interfaces generated during pyrolysis reorganize local charge distribution, lower energy barriers, and speed up surface reaction kinetics. [27]. Dong *et al*. demonstrated that treatment with alkaline activators such as KOH, K_2CO_3, $KHCO_3$, and CH_3COOK substantially enhances the surface area and pore development of microalgae-derived carbons. [28]. Their results underscore the decisive role of alkaline activation in governing textural evolution throughout the pyrolysis process, as illustrated in Figure **1a**. As the amount of heteroatom-enriched defects, hierarchical pores, and metal–carbon contacts increases, catalytic performance strengthens accordingly. Because pyrolysis adjusts graphitization, defect creation, and pore development simultaneously—rather than precisely controlling composition as in wet-chemical methods—its optimization requires balancing conductivity, defect density, and mass-transport features to achieve synergistic enhancement of intrinsic activity and overall efficiency.

2.2. Hydrothermal Carbonization Methods

Hydrothermal carbonization (HTC) provides an alternative and widely adopted route for transforming algae and other moisture-rich biomass into carbonaceous

catalyst materials. In contrast to conventional pyrolysis, HTC proceeds under comparatively mild hydrothermal conditions (typically 180–250 °C), which promotes the preservation of spherical morphologies and the retention of oxygen-containing functional groups during carbon formation. These attributes enable the production of hydrochar with controllable particle size and surface chemistry. However, HTC-derived carbons generally exhibit low intrinsic porosity and thus often require subsequent chemical activation to establish a hierarchical pore architecture suitable for electrocatalytic applications. Overall, HTC offers an energy-efficient, morphology-retentive route that complements conventional high-temperature pyrolysis and activation strategies.

2.3. Wet-Chemical Methods

Another strategy often used by many researchers is protein-assisted sol–gel synthesis. The sol–gel method allows the production of nanocrystalline materials with well-controlled chemical composition and particle size [29,

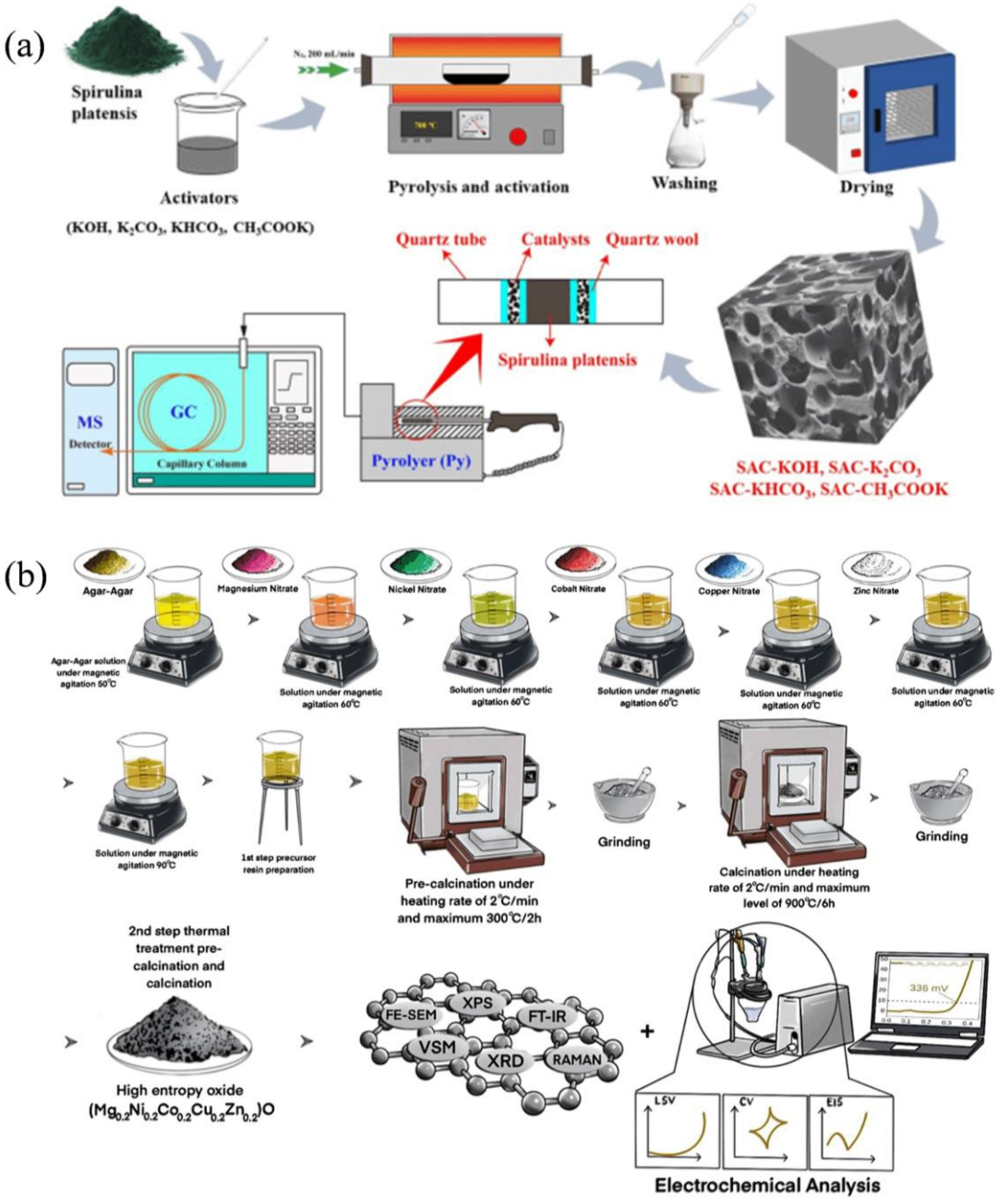

Figure 1: Synthesis process of (a) the SAC–KOH catalyst via a pyrolysis-based activation route. Ref. 28. Copyright 2025, Elsevier. and (b) the $Mg_xNi_xCo_xCu_xZn_xO$ catalyst obtained through a sol–gel-assisted method. Ref. 34. Copyright 2024, Elsevier.

30]. This method has several advantages, including simplicity, low cost, fast processing, and reduced amount of waste harmful to the environment [31]. Usually, this method starts with the preparation of a colloidal solution, followed by polymerization reactions to form an amorphous network, which later undergoes hydrolysis to form a gel [32]. Finally, drying and further processing provide the desired material. Commonly used gels are gelatin and agar. Because of their non-toxicity, excellent biodegradability, and good compatibility with life, such gels in recent years have been widely used as polymer additives in the synthesis process [33]. Jakeline *et al*. employed the sol–gel method to extract agar from RA, as shown in Figure **1b** [34]. The agar served as a polymeric agent in synergy with transition metals to synthesize a high-entropy oxide, $Mg_XNi_XCo_XCu_XZn_XO$ (X= 0.2). The introduction of agar promoted an increased density of oxygen vacancies, generated more active sites, facilitated single-phase formation, and enhanced charge transfer capability. As a result, the catalyst exhibited a low overpotential of 336 mV versus the reversible hydrogen electrode (vs. RHE), thereby improving its OER performance [34].

In contrast to pyrolysis, wet-chemical strategies offer far greater precision in tuning metal–oxygen coordination environments, introducing well-defined defects such as oxygen vacancies, and directing phase evolution during synthesis. Pyrolysis, on the other hand, remains advantageous for producing carbonaceous materials with extensive surface area and hierarchical porosity. Broadly comparing these approaches, pyrolysis-derived carbons typically exhibit superior electrical conductivity and a high density of defect sites, whereas sol–gel-generated oxides enable fine regulation of elemental composition and crystallographic order. Consequently, the choice of synthetic route should be guided by the nature of the desired catalytic centers—whether carbon defects, heteroatom functionalities, or metal–oxygen frameworks—and by the required balance among conductivity, porosity, and intrinsic active-site reactivity.

While both pyrolysis and sol–gel approaches can introduce heteroatoms and restructure the material framework, the intrinsic strengths of algal biomass as a precursor warrant clearer recognition. In contrast to lignocellulosic or agricultural biomass, which is largely restricted to carbon and oxygen, algae inherently contain high levels of nitrogen, sulfur, phosphorus, and silicon originating from proteins, amino acids, and mineral assimilation. Upon thermal treatment, these heteroatoms are directly transformed into pyridinic-N, graphitic-N, thiophene-S, and Si–C moieties, enabling efficient self-doping without external dopant sources. These biochemical and structural inheritances set algae apart from traditional biomass, giving rise to higher defect densities, improved heteroatom retention, well-developed porosity, and strengthened metal–biomass electronic coupling. Consequently, the superior catalytic properties of algae-derived materials arise not merely from post-synthetic activation but fundamentally from the inherent elemental composition and bioarchitecture of algae, which jointly dictate the electronic structure, active-site accessibility, and overall electrocatalytic performance.

3. ELECTROCATALYTIC APPLICATIONS OF ALGAE-DERIVED ELECTROCATALYSTS

3.1. Oxygen Reduction Reaction (ORR)

Oxygen reduction reaction (ORR), as one of the key processes in fuel cells and metal–air batteries, is severely limited by sluggish kinetics and large overpotentials at the cathode [35]. Hence, the development of efficient catalysts is essential to improve ORR conversion efficiency [36]. Carbon is widely employed as a carrier for electrochemical energy conversion in fuel cells and related systems, and carbon-based materials have been demonstrated to play a vital role in enhancing the catalytic performance of ORR [37, 38]. In this context, algae-derived biomass, as a natural carbon source with advantages of abundance, low cost, and renewability, has recently been extensively explored for the synthesis of efficient ORR catalysts.

3.1.1. Microalgae-derived Electrocatalysts for ORR

In recent years, MA have attracted considerable attention in the field of electrocatalysis as a renewable carbon source, owing to their abundance of nitrogen-containing biomolecules and unique cellular architecture [39-41]. MA can readily form porous carbon structures during pyrolysis, simultaneously enabling effective nitrogen doping [42]. These features make them highly promising precursors for the development of ORR catalysts.

Ma *et al*. developed a two-step strategy, involving pyrolysis and nitrogen doping, to upgrade MA into single-atom catalysts (SACs) [43] and eventually raised the temperature to 900 degrees (malg-SAC-900).[43]. As illustrated in Figure **2a**, MA-derived biomass was first obtained through photosynthesis and subsequently converted into hydrothermal carbon via a hydrothermal treatment process. This intermediate was then ultrasonically mixed with a nitrogen precursor under an

inert N_2 atmosphere, followed by pyrolysis to form malg-SAC. The structural evolution of the samples was analyzed by Raman spectroscopy, as shown in Figure **2b**. Raman spectra revealed that with increasing pyrolysis temperature (up to 900 °C), the degree of disorder in the carbon structure increased, as indicated by the rising ID/IG ratio. The Raman analysis reveals a progressive restructuring of the carbon matrix throughout pyrolysis, accompanied by the efficient integration of heteroatoms into the evolving framework. In summary, this work demonstrates that the two-step synthesis route facilitates the formation of atomically dispersed Fe sites and a highly porous structure, which collectively enhance the ORR activity. Compared with commercial Pt/C and other activation strategies, malg-SAC-900 exhibits superior ORR performance with a $E_{1/2}$= 0.875 V vs. RHE [44].

Wang *et al.*, achieved nitrogen enrichment of MA by lipid extraction to synthesize microalgae carbon (MAC) and microalgae residue carbon (MRC) [45]. As shown in Figure **2c**, the time-resolved 3D FTIR spectra indicate the generation of NH_3 and HCN during pyrolysis. These volatile nitrogen-containing species act as in situ activating agents, contributing to increased specific SBET and a higher degree of graphitization, while concurrently promoting nitrogen incorporation into the evolving carbon framework. Figure **2d** further confirms that the nitrogen content in the MR sample is significantly higher than that

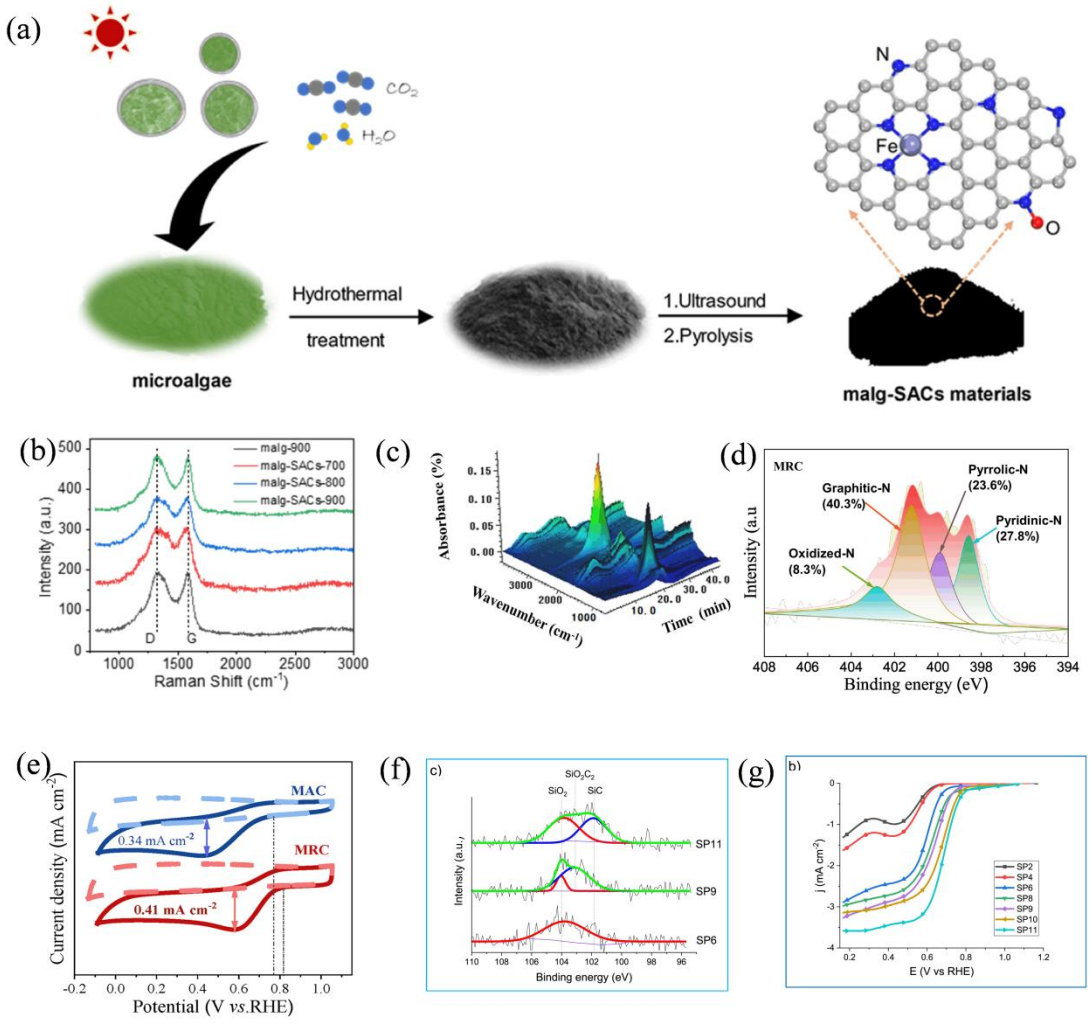

Figure 2: (a) Schematic illustration of the synthesis of the malg-SAC catalyst via pyrolysis. (b) Raman spectra of the malg-SAC catalyst Ref. 43. Copyright 2023, Elsevier. (c) Three-Dimensional (3D) Fourier-transform infrared spectroscopy (FTIR) spectra of the malg-SAC catalyst. (d) XPS spectra of the malg-SAC catalyst. (e) Cyclic Voltammetry curve curves (CV) of the malg-SAC catalyst Ref. 45. Copyright 2022, Elsevier. (f) Silicon self-doped biochar: the SP-11 sample synthesized via Pyrolysis Methods. X-ray Photoelectron Spectroscopy (XPS) spectra of the SP-11. (g) Linear sweep voltammetry (LSV) curves of SP-11 at 1600 rpm, O_2-saturated, with a scanning rate of 10 mV s^{-1} Ref. 49. Copyright 2025, Elsevier.

in MA, indicating that protein enrichment effectively promotes nitrogen accumulation. High-resolution N 1s spectra reveal that nitrogen in the catalyst predominantly exists in the forms of pyridinic-N, graphitic-N, pyrrolic-N, and oxidized-N. Based on previous studies and theoretical insights, pyridinic-N and graphitic-N are widely recognized as the key active sites for enhancing ORR activity. Compared to other samples, the f-MAC sample exhibits a higher proportion of these two species, which contributes to improved catalytic performance, suggesting that tailoring the nitrogen species distribution can effectively optimize ORR activity. As shown in Figure **2e**, the MRC sample demonstrates a higher current density and a more positive onset potential than MAC, indicating superior ORR catalytic activity. Moreover, the MRC exhibits a $E_{1/2}$= 0.72 V vs. RHE, which is notably higher than that of MAC. This enhanced performance is primarily attributed to the higher nitrogen doping level in MRC, especially the increased content of graphitic-N and pyridinic-N, which are considered the dominant active sites for ORR. In summary, MA-based catalysts exhibit excellent electrochemical performance for the ORR. The introduction of nitrogen dopants effectively modulates the electronic structure, thereby enhancing ORR activity. These findings are consistent with the performance trends outlined in Table **1**, which shows that the most efficient catalysts typically possess high heteroatom incorporation and well-developed porous architectures derived from algal precursors.

In summary, electrocatalysts derived from MA show excellent electrochemical performance in the ORR. This high activity mainly results from their nitrogen-rich composition, hierarchical porous structure, and flexible, adjustable electronic configuration. During pyrolysis, the carbon and nitrogen sources inside MA are converted into highly conductive carbon frameworks with numerous defect sites, thereby exposing more active centers. In particular, the introduction and control of pyridinic-N and graphitic-N species effectively optimize the local electronic environment, facilitating oxygen adsorption and accelerating electron transfer. Overall, MA-derived catalysts combine structural advantages with electronic modulation effects, showing high half-wave potentials and outstanding synergistic catalytic activity. These properties emphasize the great potential of MA-derived carbon materials for clean energy conversion applications.

3.1.2. Sargassum spp.-derived Electrocatalysts for ORR

In recent years, SP, a brown macroalga widely distributed in coastal regions, has attracted increasing attention as a promising precursor for ORR electrocatalysts due to its high carbon content and natural abundance of heteroatoms such as silicon and nitrogen [46]. Its unique biological architecture facilitates the formation of a porous structure, which provides favorable pathways for mass transport and exposure of active sites during the ORR process [47]. Recent studies have demonstrated that structural properties can be effectively tailored through thermal treatment and activation strategies, thereby endowing SP-derived carbon materials with excellent ORR electrocatalytic performance [48].

Isaias *et al*. employed a thermal treatment SP as the carbon source. The silicon precursors—SiO_2, $Si(OH)_4$, and atoms naturally adsorbed within the algal biomass—enabled the construction of silicon self-doped biocarbon in a one-step synthesis [49]. To investigate the effect of pyrolysis temperature on the specific surface area and ORR performance, N_2 physisorption analyses were conducted on biocarbon samples prepared at different temperatures (SP6, SP9, and SP11). According to Figure **2f**, the Si 2p XPS spectra reveal binding energies at 101.8 eV, 103.0 eV, and 104 eV, corresponding to Si–C, SiO_2C_2, and SiO_2, respectively. The results indicate that at 600 °C, silicon remains primarily in its oxidized form (SiO_2 or $Si(OH)_4$). Under natural conditions, silicon and oxygen usually exist together [50]. Upon increasing the temperature to 900 °C and 1100 °C, a progressive transformation occurs, wherein Si–C bonding is formed through the thermal decomposition of SiO_2 and $Si(OH)_4$. This suggests that high-temperature treatment facilitates the detachment of oxygen atoms, generating reactive sites that promote the formation of Si–C bonds [51]. Consequently, elevated pyrolysis temperatures enhance the incorporation of silicon into the carbon lattice, thereby modulating the electronic structure and improving catalytic properties [52]. Previous studies have shown that the incorporation of heteroatoms into the biocarbon matrix can significantly enhance ORR activity [53]. Specifically, silicon doping contributes to improved electron transport between adjacent silicon sites [54]. As illustrated in Figure **2g**, LSV reveals that the sample treated at 1100 °C exhibits the most favorable ORR performance, with an onset potential (E_{oneset}) of 0.82 V and a half-wave potential ($E_{1/2}$) of 0.68 V vs. RHE. These findings demonstrate that the structural evolution of SP-derived biocarbon induced by thermal activation enhances the exposure and integration of silicon atoms within the carbon framework, thereby improving electrocatalytic activity. This observation is consistent with previous literature reports [55].

Escobar *et al*., utilized SP, a brown macroalga collected from Caribbean beaches, as both a carbon and nitrogen source to synthesize N-doped carbon materials. Standard untreated (RS), pyrolysis at 700 ℃ for 90 minutes (SPY), drying at 80℃ overnight (SDO) through pyrolysis, doping, and activation treatments [56]. As shown in Figure **3a**, the pristine SP surface exhibits uniformly distributed square-shaped macropores. After pyrolysis, the SPY sample shows an irregular aggregated structure with some blocked pores Figure **3b**, which results in a reduction of the BET surface area of RS. As illustrated in Figure **3c**, the SBET, calculated via the BET equation from N_2 adsorption–desorption isotherms, demonstrates that different processing methods have a pronounced effect on the structural characteristics of SP-derived carbons. The RS sample obtained by pyrolysis alone shows a significant decrease in SBET from 34.42 $m^2 g^{-1}$ to 3.86 $m^2 g^{-1}$, primarily due to the collapse and blockage of pores by volatile components, as confirmed by SEM observations. In contrast, the solvothermal treatment effectively increases SBET by generating small aggregates, resulting in a micropore-dominated structure with the SDO sample achieving the highest surface area of 133.87 $m^2 g^{-1}$ among all samples. These results indicate that the activation process efficiently promotes the development of a porous structure. SEM and BET analyses reveal that the activated samples exhibit rougher surfaces with improved porosity and pore size distribution. The creation and enhancement of porous architectures expose more active sites and facilitate mass transport during the ORR [57]. Overall, the study demonstrates that the combination of pyrolysis, doping, and activation yields three catalysts with excellent ORR performance. In particular, the SDO sample not only possesses the highest SBET (133.87 $m^2 g^{-1}$) but also exhibits the most positive onset potential (0.852 V vs. RHE), confirming its superior ORR catalytic activity.

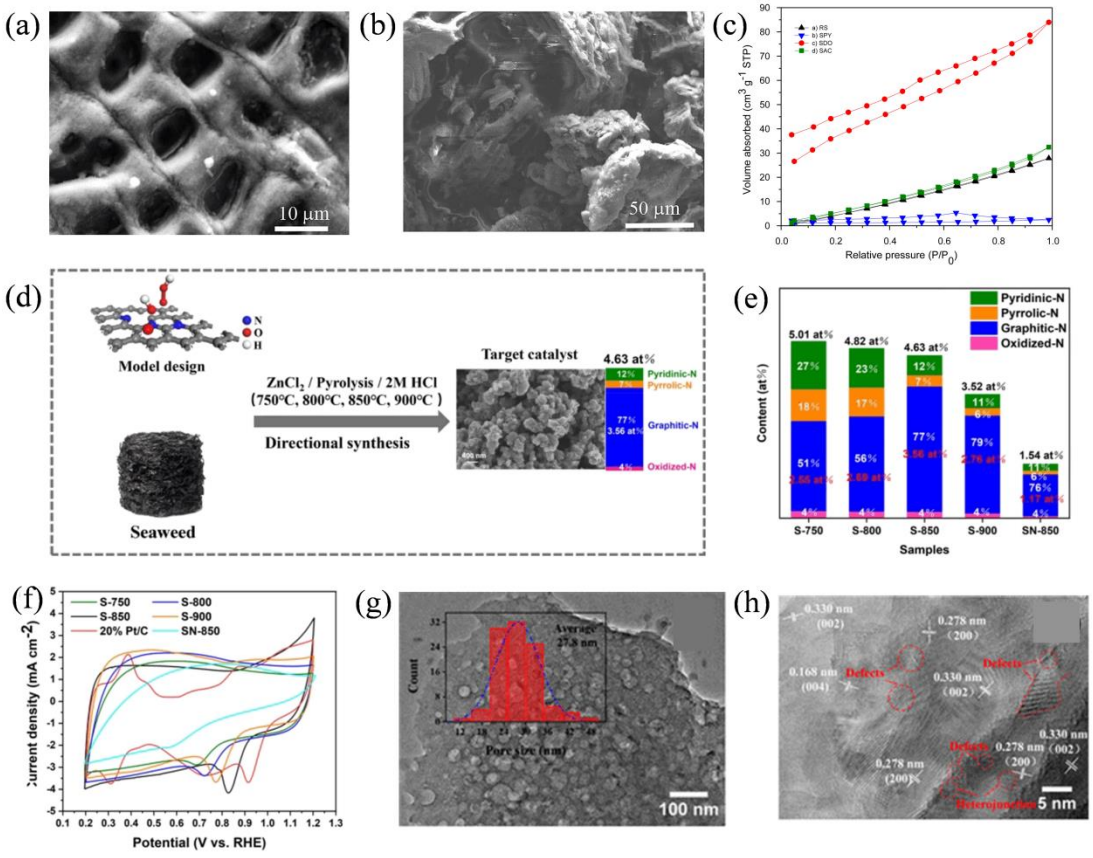

Figure 3: The RS, SPY, SDO, and SAC specimens prepared through via pyrolysis method (a) Scanning electron microscope (SEM) micrographs of RS materials (b)SEM micrographs of SAC materials. (c) nitrogen adsorption/desorption isotherms of RS, SPY, SDO, SAC Ref. 56. Copyright 2017, Elsevier. (d) Illustration of the synthesis of the S-850 catalyst obtained via pyrolysis in the temperature range of 750–900 °C. (e) Total doping N atom content and the function-N atom ratio of S-750 to S-900. (f) CV curves of the S-850 catalyst via pyrolysis method. Ref. 62. Copyright 2025, Springer. Transmission electron microscopy (TEM) images of (g) PBC-7 00 and (h) PBC-800 Ref. 65. Copyright 2019, American Chemical Society.

In summary, ORR catalysts derived from SP exhibit several intrinsic advantages. First, SP is naturally enriched with silicon and nitrogen, enabling in situ heteroatom self-doping during thermal treatment without the need for additional precursors. Moreover, silicon incorporation tunes the electronic structure through a mechanism distinct from nitrogen doping. While pyridinic- and graphitic-N enrich the surrounding carbon lattice by donating lone-pair electrons, Si–C bonding drives a downward shift of the carbon p-band center and promotes greater electron delocalization, thereby enhancing electrical conductivity and reinforcing O_2 adsorption. This complementary electronic modulation provides further insight into the superior ORR performance observed for SP-derived carbons. This not only simplifies the synthesis process but also reduces overall production costs. Second, high-temperature pyrolysis and activation processes facilitate the development of porous structures with large specific surface areas, which significantly enhance the exposure of active sites and improve mass transport efficiency during the ORR process [58]. Overall, SP-derived carbon materials possess inherent advantages in structural tunability, active site integration, and electrical conductivity enhancement, making them promising candidates for the development of environmentally friendly, cost-effective, and high-performance ORR electrocatalysts.

3.1.3. SW-derived Electrocatalysts for ORR

SW, which is rich in proteins, possesses a relatively high nitrogen content [59]. In recent years, it has frequently been employed as a precursor for heteroatom-doped carbon catalysts through pyrolysis and activation. SW not only enables the self-doping of nitrogen into the carbon framework but also promotes the formation of graphitic-N and pyridinic-N species, which have been widely recognized in previous studies as the key active sites for the ORR[60, 61].

Zhang *et al*. increased the ratio of graphitic-N to total N atoms from 46% to 80% by elevating the pyrolysis temperature, while the overall nitrogen content decreased from 5.01 at% to 3.52 at% [62]. It can be seen that seaweed, as an excellent biomass precursor, has a natural nitrogen-containing organic matter structure. The (Figure **3d**) model design shows that seaweed has a nitrogen-doped carbon skeleton (containing pyridinic nitrogen, pyrrolic nitrogen, graphitic nitrogen, etc.). [63]. According to earlier studies, the total doped nitrogen tends to volatilize at elevated temperatures, whereas the proportion of graphitic-N gradually increases. As shown in Figure **3e**, self-doped porous carbon ORR catalyst (S-850) represents a balance between the proportion of graphitic-N and the total nitrogen content among the samples. Notably, it exhibited the highest graphitic-N content (3.65 at%) among these catalysts. As evidenced by the LSV and CV results in Figure **3f**, under identical conditions, S-850 exhibits a markedly higher peak than the other samples, indicating its superior ORR activity. These results demonstrate that a higher graphitic-N content leads to a lower ORR energy barrier and provides a theoretical structural advantage [64].

Similarly, Li *et al*. employed SW as a precursor to synthesize a multifunctional, nitrogen-rich porous biochar (PBC-800) through carbonization and activation [65]. As shown in Figure **3g**, the surface of the obtained sample exhibits abundant pores with average pore sizes of approximately 27.8, 17.1, and 20.1 nm. The material displays a honeycomb-like carbon framework, which not only provides excellent electronic conductivity but also exposes numerous defects, as illustrated in Figure **3h** [66]. The results indicate that nitrogen-rich SW can be self-doped into mesoporous carbon, generating numerous defects and active sites. [67].

According to previous reports, porous carbon materials derived from SW as a precursor often feature well-developed nitrogen configurations, abundant active sites, and interconnected mesoporous networks [68]. These structural characteristics effectively reduce the energy barrier for the ORR, thereby delivering excellent electrocatalytic performance.

In summary, the three types of algae-derived electrocatalysts—MA, SW, and SP—show distinct advantages in the ORR. MA catalysts have a nitrogen-enriched structure that allows in situ nitrogen incorporation during pyrolysis and the formation of atomically dispersed Fe–N_x active centers, optimizing the electronic structure and accelerating reaction kinetics. SW catalysts, characterized by their high protein content, easily form various nitrogen species such as pyridinic-N and graphitic-N. By adjusting the proportion of graphitic-N, hierarchical porous structures can be created that improve conductivity and reveal more active sites. SP catalysts introduce silicon and nitrogen heteroatoms into the carbon framework simultaneously, forming Si–C networks that facilitate charge transfer and generate well-developed mesoporous structures through the synergistic effect between Si and N. These properties effectively lower the ORR energy barrier and enhance catalytic durability. These advantages not only provide naturally renewable catalyst sources for fuel cells and metal–air

batteries but also contribute to the sustainable reutilization of waste algal biomass. Importantly, MA and SW precursors exhibit markedly different structural features. MA, with its greater protein and nitrogen content, preferentially generates pyridinic- and graphitic-N functionalities during pyrolysis. In contrast, SW contains higher levels of inorganic constituents such as Si, S, and various metal ions, enabling multi-heteroatom co-doping and fostering the formation of hierarchical porous architectures. To enhance the continuity of the discussion, a brief comparison is introduced here. MA predominantly utilizes nitrogen-rich biomolecular precursors to form Fe–N_x motifs or N-doped active sites, whereas SP benefits from Si–C incorporation and silicon-mediated electronic modulation. In contrast, SW-derived carbons achieve improved ORR activity mainly through protein-derived nitrogen species and the generation of graphitic-N. These distinctions underscore how variations in algal biochemica composition give rise to different active-site configurations and subsequently distinct ORR mechanisms.

3.2. Oxygen Evolution Reaction (OER)

The OER, as one of the key half-reactions in water splitting and metal–air batteries, is a complex multistep process involving a sluggish four-electron transfer [69]. To date, Ru, Ir, and their alloys are recognized as benchmark OER catalysts [70]. In recent years, catalysts derived from waste algal biomass have attracted increasing attention owing to their high efficiency, stability, and economic sustainability, providing significant advances for OER catalysis and clean energy conversion.

3.2.1. SW-derived Electrocatalysts for OER

SA is a polysaccharide derived from marine biomass and extracted from SW, has recently attracted increasing attention as a promising precursor for OER catalysts [71]. Upon appropriate processing, SA offers abundant functional groups that provide a versatile platform for the incorporation of transition metals and heteroatoms. In addition, its inherently high surface area and tunable electronic structure make it an ideal candidate for constructing advanced catalytic systems. These features collectively offer valuable insights into the rational design of efficient OER electrocatalysts.

Yang *et al*., synthesized a 3D hierarchical aerogel catalyst, Ni/NiO/$NiCo_2O_4$/N-CNT-As hybrid, through an ion-exchange process followed by pyrolysis of sustainable SA [72]. Benefiting from its unique 3D architecture as shown in Figure **4a**, the material exhibits a highly porous framework that facilitates charge transfer at the catalytic centers, while the interconnected hierarchical mesoporous hybrid structure enables efficient mass transport. As shown in Figure **4b**, in 1 M KOH the ternary Ni/NiO/$NiCo_2O_4$/N-CNT-As catalyst exhibits a remarkably low onset potential of 1.43 V vs. RHE, which is lower than that of the binary counterparts and commercial IrO_2/C. Moreover, it delivers a significantly higher current density compared with other aerogel samples, highlighting its superior OER activity. As presented in Figure **4c**, all aerogel samples display relatively low Tafel slopes, among which Ni/NiO/$NiCo_2O_4$/N-CNT-As achieves the lowest value. In contrast to conventional porous supports, the reduced Tafel slope of Ni/NiO/$NiCo_2O_4$/N-CNT-As aerogel catalysts indicates enhanced catalytic kinetics afforded by the novel aerogel architecture.

Dong *et al*., employed sodium lignosulfonate and SA as carbon precursors, and synthesized a P-Ru/SC-2 catalyst by anchoring Ru clusters onto S-doped carbon aerogels (P-Ru/SC) through a novel plasma-assisted high-temperature carbonization process, as illustrated in Figure **4d-e** [73]. In 1 M KOH, the P-Ru/SC-2 catalyst with S coordination and P doping exhibits the lowest charge-transfer resistance (Rct), confirming its superior electron transport capability among the tested samples. Moreover, the synergistic effect of graphitized carbon and stable Ru–S bonds significantly accelerates the reaction kinetics, thereby enhancing the OER performance. Notably, P-Ru/SC-2 achieves the lowest overpotential of 193.4 mV at 10 mA cm^{-2}, outperforming Ru/SC-1, which demonstrates that P-Ru/SC-2 possesses the most favorable catalytic activity toward OER.

In summary, SA has been demonstrated to be an efficient biomass precursor [74]. The results reveal that aerogel catalysts derived from SA endow the materials with unique structural and electronic advantage, thereby significantly enhancing their OER activity.

3.2.2. RA-derived Electrocatalysts for OER

RA, as a valuable marine biological resource, are rich in polysaccharides such as agar and carrageenan[74]. Agar not only serves as an excellent carbon precursor but also acts as a structural directing agent in sol–gel systems, thereby optimizing catalyst morphology and increasing the density of surface active sites [75]. In recent years, agar extracted from RA has been successfully employed for the synthesis of transition metal oxides as OER catalysts, which markedly enhance the reaction kinetics of the oxygen evolution reaction.

Jakeline *et al*., extracted agar from RA and utilized it as a polymeric agent to synthesize $MnxCo_{3-x}O_4$ via a protein sol–gel method [76]. In this study, the Mn content was carefully controlled, and it was observed that increasing the Mn concentration led to a higher proportion of Mn^{2+} oxidation states dominating the surface composition. Moreover, the O_2/O_1 ratio was found to increase progressively with the Mn content. As shown in Figure **4f–g**, the sample with $MnCo_2O_4$ (x = 1.0) exhibited the highest OER activity, delivering the lowest overpotential (299 mV) along with the smallest Tafel slope (52 mV dec^{-1}). This superior performance is attributed to the introduction of Mn, which increased the defect density within the structure, thereby enhancing the number of surface-active sites, facilitating mass transport, and accelerating the OER kinetics. These results are consistent with previous reports [77].

Daniel *et al*., employed agar extracted from RA to synthesize $CoFe_2O_4$ via a protein sol–gel method [78]. As shown in Figure **4h**, at an overpotential of 400 mV vs. RHE, the TOF of the agar-derived CoFe2O4 (8.8×10^{-2} s^{-1}) was markedly higher than that of the gelatin-derived counterpart (1.9×10^{-3} s^{-1}). The superior activity of the agar-based material indicates that the increased number of surface active sites significantly promotes the OER kinetics. Under alkaline conditions (1 M KOH), stability measurements conducted using multi-step chronopotentiometry (Figure **4i**) demonstrated that the electrode exhibited excellent catalytic and mechanical stability during the OER process. Moreover, the agar-derived $CoFe_2O_4$ achieved a lower overpotential of 360 mV vs. RHE at 10 mA cm^{-2} compared to the gelatin-derived counterpart (435 mV vs. RHE). These results clearly indicate that agar extracted from RA provides a more favorable substrate for enhancing the OER catalytic activity of $CoFe_2O_4$ than gelatin.

Overall, these studies demonstrate that agar extracted from RA endows transition metal oxides with a tunable

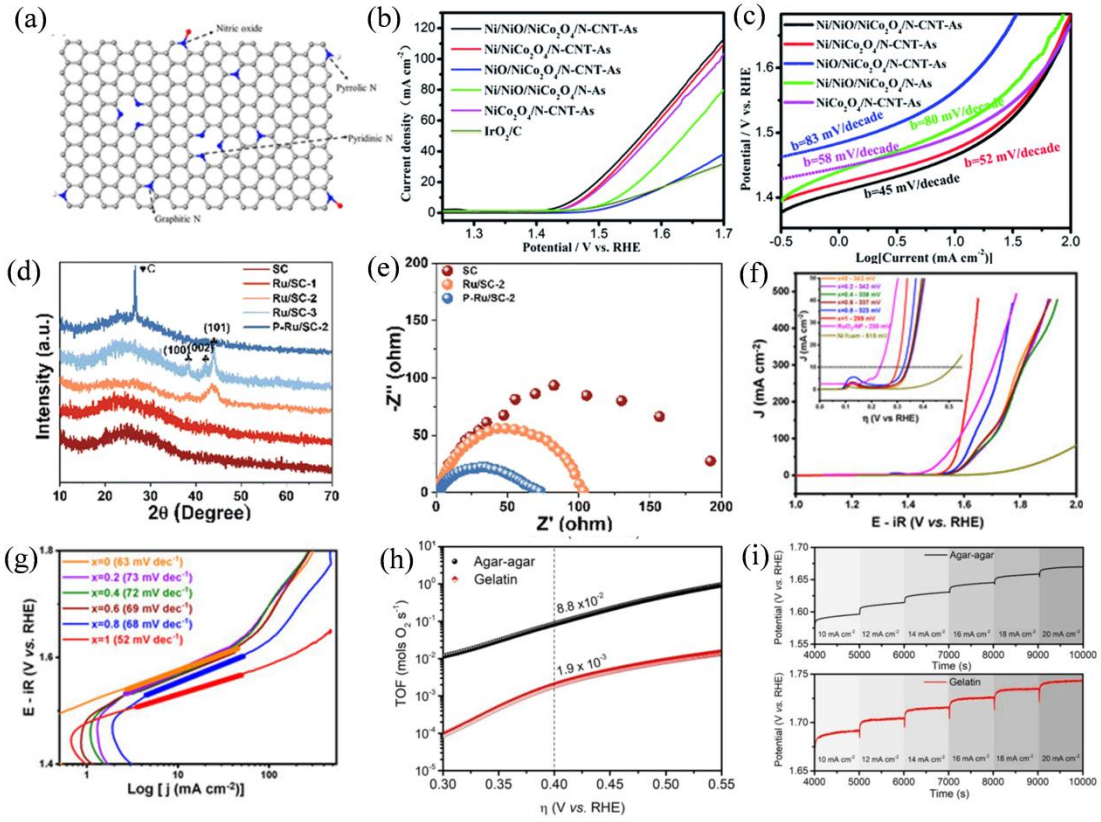

Figure 4: (a) 3D structure of PBC-800.Morphology of Ni/NiO/$NiCo_2O_4$/N-CNT-As. Copyright 2019, American Chemical Society. (b) LSV curves and (c) corresponding Tafel slopes Ref. 72. Copyright 2019, Royal Society of Chemistry. (d) schematic illustration of the synthesis strategy for P-Ru-SC-2. (e) EIS plots of SC, Ru/SC-2, and P-Ru-SC-2. Copyright 2024, Royal Society of Chemistry Ref. 73. (f) lsv curves and (g) tafel slopes of $MnxCo_{3-x}O_4$ (x = 0-1) Ref. 76. Copyright 2022 Multidisciplinary Digital Publishing Institute. (h) TOF values of $CoFe_2O_4$. (i) Multi-step chronopotentiometry tests were performed on $CoFe_2O_4$ powders obtained from agar and gelatin at different current densities Ref. 78. Copyright 2019, Elsevier.

specific surface area and defect regulation capability. The increased exposure of active sites effectively accelerates the OER kinetics, thereby providing new insights into the extraction of polysaccharides from RA and their application as substrates for catalyst synthesis.

Two types of algae-derived electrocatalysts—SA and RA—show great potential in the oxygen evolution reaction (OER), each functioning through distinct mechanisms. SA, a polysaccharide derived from brown algae, can be transformed into three-dimensional porous aerogel structures through carbonization. This structure has a large specific surface area and good conductivity, facilitating charge and mass transport. The introduction of transition metals further optimizes the interfacial electronic structure and accelerates reaction kinetics, while heteroatom incorporation strengthens synergistic effects. Meanwhile, RA catalysts are mainly obtained via sol–gel systems that act as both pore-forming templates and carbon sources, also incorporating transition metals. Their high defect density and metal synergy improve adsorption–desorption processes, thus enhancing OER kinetics. Overall, SA catalysts rely on conductive 3D architectures and heteroatom synergy, whereas RA systems achieve a high density of active sites through sol–gel chemistry and defect engineering. In recent years, algae have been widely used as sustainable and low-cost precursors for large-scale catalyst production, improving catalytic activity and selectivity while promoting the reuse of waste biomass. In contrast to SA-derived aerogels, which primarily leverage three-dimensional conductive architectures, RA-based catalysts rely more extensively on sol–gel–driven defect engineering and tunable metal–oxide coordination environments. This represents a complementary strategy for enhancing OER performance.

3.3. Other Reactions

Compared with ORR and OER, reactions such as HER, CO_2RR, and NO_3RR are more directly associated with environmental remediation and clean energy conversion [79]. HER plays a pivotal role in the sustainable production of hydrogen as a clean energy carrier [80]. CO_2RR offers a promising route to convert CO_2 into value-added energy products, which is of great significance since CO_2 is a major greenhouse gas closely linked to global climate change and environmental issues [81]. In line with sustainable development strategies, both the reduction of CO_2 emissions and its efficient utilization are of critical importance. Meanwhile, NO_3RR provides an effective approach for the remediation of nitrogen-based fertilizers such as urea ($CO(NH_2)_2$) and ammonia (NH_3), thereby alleviating the pressing challenges associated with perturbations of the natural nitrogen cycle [82, 83]. In recent years, algae have been increasingly exploited to develop low-cost and scalable catalysts to enhance the activity and selectivity of these reactions, not only improving catalytic efficiency but also achieving the reutilization of waste algal biomass.

3.3.1. Harmful Algal Blooms–derived Electrocatalysts for HER/CO_2RR

HABs frequently occur in aquatic ecosystems worldwide, posing severe threats to the environment, water ecology, and human health [84]. The biomass of HABs is enriched with carbon (CO_2) and essential nutrients such as N and P, offering new opportunities for environmental remediation and the development of sustainable energy strategies [85, 86]. In recent years, researchers have explored the conversion of HABs into catalysts and discovered their potential in facilitating C–N coupling reactions for catalyst design.

Yan *et al*. employed a wet/sonochemical approach followed by annealing to convert HABs into the Cu_1Mo_1/NC catalyst [87]. As shown in Figure **5a–b**, the XRD pattern of Cu_1Mo_1/NC exhibits characteristic peaks of hexagonal MoN, with no diffraction peaks corresponding to Cu species. Furthermore, in situ XRD confirmed the emergence of MoN reflections after annealing at 500 °C. With increasing annealing temperature, these diffraction peaks became more pronounced. As shown in Figure **5c**, the adjacent lattice spacings of 0.249 and 0.172 nm correspond well to the (200) and (202) planes of hexagonal MoN. Moreover, the proportion of pyridinic N and pyrrolic N decreased with higher annealing temperature, indicating their involvement in the formation of MoN. Consequently, no Mo oxides were detected on the catalyst surface, suggesting that the intrinsic nitrogen from HABs directly participated in the MoN formation process. This study achieved the NO_3RR and CO_2RR. As shown in Figure **5d**, t On the Cu_1Mo_1/NC catalyst, the adsorption energy of $*NO_3$ (−3.90 eV) is greater than that of $*CO_2$ (−3.55 eV), indicating a stronger affinity for nitrate species. The energy barrier for $*NO_3H \rightarrow *NO_2$ (0.86 eV) is lower than for CO_2 reduction, suggesting that nitrate reduction is more favorable. The in-situ ATR-FTIR spectra show that CO_2 can directly couple with *NH to form the $*NHCO_2$ intermediate, followed by the rate-determining step ($*NHCOOH \rightarrow *NHCO$, 1.11 eV) and an exothermic C–N coupling leading to urea formation. At U_{RHE} = −1.05 V, the overall free-energy curve continuously decreases, indicating a thermodynamically favorable process, while

Mo/C still exhibits a significant energy barrier, confirming that the Cu–Mo synergistic effect greatly promotes urea electrosynthesis.

Yu *et al*., proposed a thermochemical strategy to convert HABs into nitrogen-doped carbon materials, denoted as E-NC and MA-NC [88]. As shown in Figure **5e–f**, FTIR analysis of E-NC and MA-NC revealed similar spectra, indicating that these materials possess comparable surface functional groups. The bands observed at ~1100 to ~1000 cm^{-1} were assigned to the stretching vibrations of C–N or C–O. By NEXAFS analysis further revealed the nitrogen chemical states in the carbon materials, confirming that both samples possessed a similar carbon framework environment. In the N K-edge spectra, three distinct π* peaks were identified, corresponding to pyridinic N, pyrrolic N, and graphitic N, respectively. These diverse nitrogen configurations can enhance the charge transfer capability of the carbon substrate, thereby accelerating the CO_2RR kinetics.

Overall, these studies demonstrate the unique advantages of HABs in enabling C–N coupling product synthesis, offering new perspectives for the reutilization of harmful and waste algal biomass as well as for clean energy conversion. Compared with CA and MA, which primarily serve as nitrogen-rich carbon frameworks in HER and CO_2RR, HABs-derived catalysts uniquely facilitate C–N coupling owing to their inherently high nitrogen and phosphorus contents. This mechanistic distinction positions HABs as a specialized subclass of algal precursors with distinct catalytic potential.

3.3.2. CA-derived Electrocatalysts for HER/CO_2RR

CA is a representative microalga characterized by its rapid growth rate and strong nutrient uptake capacity [89,

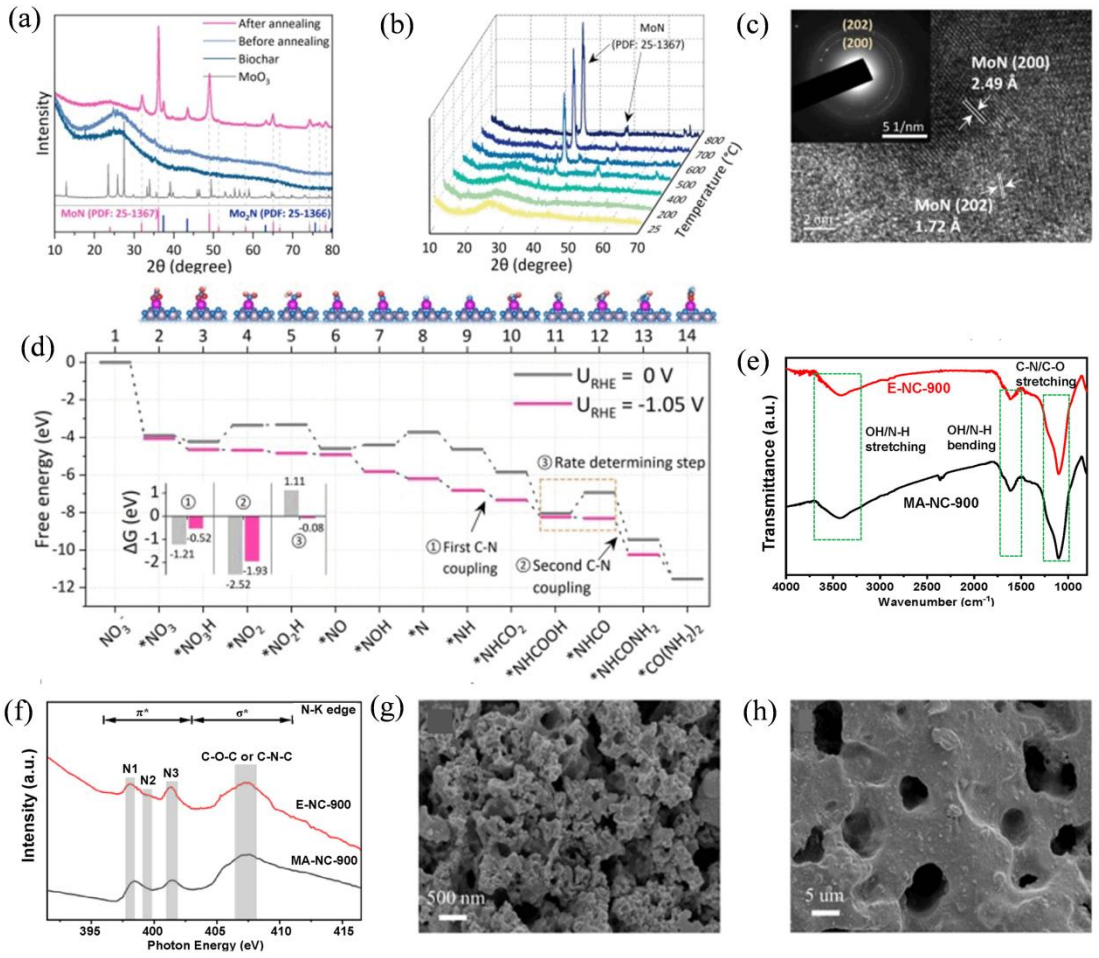

Figure 5. (a) The XRD of Cu_1Mo_1/NC, BC, and MoO_3 (b) In-suit XRD patterns of Cu_1Mo_1/NC during the reaction (c) TEM of Cu_1Mo_1/NC and selected area electron diffraction (SAEC) pattern (d) DFT calculations of free-energy diagram for urea production of Cu_1Mo_1/NC at 0 V and −1.05 V vs. RHE Ref. 87. Copyright 2024, Elsevier. (e) The FTIR of E-NC-900 and MA-NC-900 (f) N K-edge Near-Edge X-ray Absorption Fine Structure (NEXAFS) spectra of E-NC-900 and MA-NC-900 Ref. 88. Copyright 2023, American Chemical Society.(g) SEM images of CNi (h) SEM images of CNNi. Ref. 92. Copyright 2024, Elsevier.

90]. It not only provides abundant carbon and nitrogen sources but also offers a unique biomass architecture that serves as a natural template for the synthesis of high-performance catalysts [91]. In recent years, CA-derived biomass has been converted into efficient multifunctional electrocatalysts, and its remarkable electrocatalytic potential has been extensively explored.

Mei *et al*. employed CA as a biomass precursor to synthesize an N, Ni co-doped carbon-based electrode material (CNNi) [92]. As shown in Figure **5g-h**, the singly doped CNi exhibited a distinct block-like morphology. In contrast, the incorporation of both N and Ni dopants enlarged the pore size of CNNi, rendering its surface smoother and enriched with well-defined porous structures. According to the FT-IR spectra, the peak observed at 492 cm^{-1} in CNNi can be ascribed to the stretching vibration of N–Ni bonds. Compared with the singly doped samples CN and CNi, CNNi exhibited a decreased diffraction peak intensity, which may be attributed to the coordination of Ni atoms with N and O species, thereby increasing the density of surface defects in the crystal. Taken together, the results indicate that the average crystallite size of Ni in the co-doped CNNi catalyst is smaller than that in the singly Ni-doped counterpart. The reduced Ni crystallite size further confirms that CNNi possesses a larger specific surface area, thereby affording higher catalytic activity. The gaseous products detected for CNNi, CN, and CNi catalysts mainly include H_2 and CO. As illustrated in Figure **6a-b**, CNNi exhibited the highest selectivity toward CO, whereas CN and CNi catalysts showed lower CO selectivity with a pronounced tendency toward hydrogen evolution during the reduction process. Moreover, CNNi delivered a significantly higher TOF than CNi and CN, confirming that the co-doping of N and Ni not only enhanced the overall electrocatalytic reduction activity but also promoted CO formation, thereby boosting the electrode performance toward CO_2RR. Ananda *et al*., synthesized a biochar-structured material (CO@NF) using CA as the precursor [93]. As shown in Figure **6c-d**, CO exhibited a broad hump at around 23°, indicative of its amorphous nature, which is consistent with previous reports on carbonaceous materials [94]. XPS analysis further revealed that the incorporation of N dopants modified the functional groups of CO@NF. In addition, the robust carbon framework endowed the material with enhanced conductivity and electron transport capability. Under alkaline conditions (1.0 M KOH), CO@NF exhibited excellent HER catalytic performance, delivering

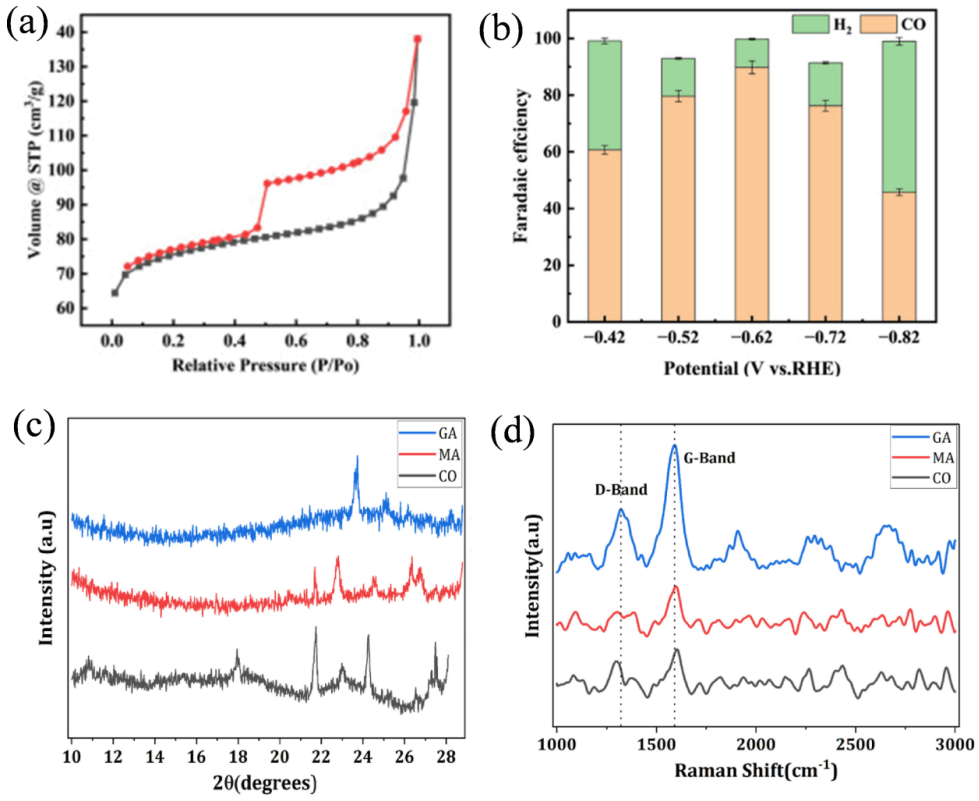

Figure 6: (a) The isothermal adsorption and desorption curves of BET for CNNi (b) Product distribution of CO_2RR by CNNi. Ref. 92. Copyright 2024, Elsevier. (c) XRD of GA, MA and CO (d) Raman of GA, MA and CO Ref. 93. Copyright 2024, Elsevier.

an overpotential of −339 mV at a current density of 50 mA cm^{-2}.

Overall, catalysts synthesized from CA biomass exhibit excellent activity and controllability toward both CO_2RR and HER. This work opens new avenues for the reutilization of CA biomass and advances the application of waste microalgae in environmental remediation.

In summary, HABs- and CA-derived electrocatalysts show excellent potential in multi-electron transfer reactions. HABs-based catalysts, enriched with nitrogen and phosphorus, achieve in situ heteroatom incorporation during pyrolysis, creating abundant active sites for C–N coupling reactions. The synergistic effect of nitrogen species facilitates interfacial formation and effectively reduces the reaction energy barrier. Meanwhile, CA-based catalysts utilize their high carbon and nitrogen content and well-organized cellular architecture as natural templates for developing porous carbon frameworks. Co-doping with transition metals forms optimized electronic structures and a high density of defects, reducing the reaction energy barrier and accelerating the kinetics. Collectively, the catalytic trends described above are consistent with the comparative results summarized in Table **1**. These characteristics not only help mitigate greenhouse gas emissions and environmental pollution but also open new pathways for sustainable energy conversion using algal biomass.

4. CONCLUSION AND PERSPECTIVES

In recent years, Algae-derived electrocatalysts have emerged as an attractive option for the design of sustainable and efficient electrocatalysts. Due to their wide distribution, rapid growth, strong nutrient absorption capacity, and intrinsic abundance of carbohydrates, proteins, lipids, as well as heteroatoms such as nitrogen, sulfur, and silicon, algae serve as ideal precursors for carbon-based catalysts [96, 97]. Through pyrolysis method, in situ heteroatom doping can be achieved, thereby generating abundant active sites [98]. For instance, pyrolysis method of MA or SP has been demonstrated to yield catalysts with low half-wave potentials.

Alternatively, the sol–gel method can be applied, in which natural polymers such as gelatin or agar are used as polymeric agents to optimize the electronic structure and thereby create efficient charge transport pathways [99]. For instance, sol–gel processing of RA has been reported to produce catalysts with low overpotentials. In recent years, increasing evidence has demonstrated that algae biomass-derived electrocatalysts exhibit excellent

Table 1: Algae-derived electrocatalysts for various electrochemical reactions.

Category	Algae	Electrocatalysts	Treating Method	Electrolyte	Performance
ORR	MA	malg-SAC-900 [95]	pyrolysis	O_2 and N_2 KOH SS[a]	$E_{1/2}$ [b] =0.875 V vs. RHE [c]
		MRC [45]	pyrolysis	O_2 and N_2 PBS SS	$E_{1/2}$ =0.72 V vs. RHE
	SP	SP11 [49]	pyrolysis	1 M KOH	$E_{1/2}$ =0.68 V vs. RHE
		SAC [56]	pyrolysis	0.5 M KOH	E_{oneset} [d]=0.838 V vs. RHE
	SW	S-850 [62]	pyrolysis	0.1 M KOH	$E_{1/2}$ =0.843 V vs. RHE
		PBC-X [65]	pyrolysis	1.69 g/L NaCl	E_{oneset} =0.838 V vs. RHE
OER	SW	Ni/NiO/$NiCo_2O_4$/N-CNT-As [72]	pyrolysis	1 M KOH	E_{oneset} =1.43 V vs. RHE
		P-Ru/Sc [73]	pyrolysis	1 M KOH	E_{10}[e]=193.4 mV
	RA	$Mn_xCo_{3-x}O_4$ [76]	wet-chemical method	1 M KOH	J_{10}[f]= 299 mV vs. RHE
		$CoFe_2O_4$ [78]	wet-chemical method	1 M KOH	J_{10}= 360 mV vs. RHE
HER/CO_2RR	HABs	Cu_1Mo_1/NC [87]	pyrolysis	0.1 M $KHCO_3$ 0.1 M KNO_3	FECO [g]= 15.2%
		MA-NC [88]	pyrolysis	CO_2 $KNOH_3$ SS	FECO= 82.7%
	CA	CNNi [92]	pyrolysis	1 M KOH	E_{100}[h]= -126 mV/s
		GA@NF [93]	pyrolysis	0.1 M $KHCO_3$	FECO= 90%

[a]SS: saturated solution; [b]$E_{1/2}$: half-wave potential for ORR; [c]RHE: reversible hydrogen electrode; [d]E_{oneset}: oneset potential for ORR; [e]E_{10}: the applied potential at a current density of 10 mA cm^{-2} for OER; [f]J_{10}: the current density of 10 mA $cm^{-2}$for OER; [g]FECO=The faradaic of CO product; [h]E_{100}= the applied potential at a current density of 100 mA cm^{-2} for HER.

performance in multi-electron transfer reactions, including ORR, OER, HER, and CO_2RR [100, 101]. These findings indicate that algae-derived catalysts hold great potential for environmental remediation and clean energy conversion. In addition, recent studies have explored the reutilization of HABs caused by excessive proliferation. The rational utilization of waste algae not only reduces ecological risks but also enables value-added use of biomass. Overall, algae-derived electrocatalysts provide a promising platform for the development of sustainable catalytic systems.

Despite the many advantages of algae-derived electrocatalysts, their application in complex multi-electron transfer reactions still faces obstacles. Issues such as limited reproducibility, insufficient structural stability, and the ambiguous identification of key catalytic centers remain major challenges. The intrinsic atomic complexity, hierarchical porosity, and coexistence of amorphous carbon phases may further obscure the precise determination of active sites. Therefore, accurate identification of catalytic centers and in-depth elucidation of their reaction mechanisms are essential for optimizing catalyst performance. To further refine future prospects, several emerging directions deserve close attention. Advanced in-situ and manipulative spectroscopy techniques provide powerful tools for studying intermediates and electronic structure reconstruction in algal-derived catalysts. Meanwhile, rational catalyst precursor design holds promise for precise control over heteroatom configurations and defect chemistry. Machine learning-aided modeling offers another avenue for accelerating carbon framework design and optimizing synthesis conditions. In this context, the following key directions for future research on algae-derived electrocatalysts are highlighted:

Understanding Reaction Mechanisms on Catalyst Surfaces

A central challenge for algae-derived electrocatalysts lies in the limited understanding of their reaction pathways and surface-active sites. The coexistence of multiple heteroatoms, hierarchical porosity, and amorphous carbon phases makes the identification of true catalytic centers highly complex [102, 103]. Future studies should integrate advanced in situ techniques and spectroscopic methods (e.g., XAS, Raman, FTIR) with theoretical approaches such as DFT to elucidate the adsorption behavior of intermediates, electron transfer mechanisms, and the correlations between structure and catalytic performance. Such insights are crucial for guiding the rational design of algae-derived electrocatalysts.

Stability and Durability Under Practical Conditions

For practical applications, long-term stability and durability remain essential challenges. Future research should focus on strategies such as protective coatings, preservation of surface structures, and structural reinforcement to enhance durability. In addition, systematic evaluations of catalyst stability under diverse conditions—such as varying temperatures, electrolytes, and applied potentials—are required to ensure their feasibility for real-world applications.

Scale-up and Integration into Practical Systems

Successfully translating algae-derived catalysts from laboratory design to practical devices is a critical challenge. Transitioning from lab-scale conditions to large-scale applications requires the development of scalable synthesis methods, cost-effective processing techniques, and standardized testing protocols to ensure both feasibility and reproducibility. Moreover, their integration into real devices—such as fuel cells, water-splitting systems, and CO_2 electrolyzers—must be carefully evaluated to determine whether their practical performance can match or surpass the outcomes demonstrated under laboratory conditions.

Machine Learning -assisted Design of Algae-derived Catalysts

Machine learning (ML) offers new opportunities for the design of algae-derived electrocatalysts. By integrating experimental data with computational prediction frameworks, ML can evaluate and optimize synthesis parameters, structural features, and precursor selection. In this way, ML can serve as a powerful tool for the efficient prediction, screening, and optimization of algae-derived catalysts.

Sustainable Synthesis and Industrial Application of Algae-derived Catalysts

Sustainability should always be a primary objective in the design of algae-derived electrocatalysts. The rational utilization of waste and harmful algae not only reduces environmental damage but also transforms them into high-value raw materials, such as feedstocks for clean energy. Future research should focus on energy-efficient, low-emission, and environmentally friendly synthesis processes. At the same time, catalyst design should be integrated with life cycle assessment (LCA) and techno-economic analysis (TEA) to evaluate their feasibility for industrial-scale applications.

CONFLICT OF INTEREST

The authors declare no conflict of interest.

FUNDING

The authors declare that this research did not receive any specific grant from funding agencies in the public, commercial, or not-for-profit sectors.

REFERENCES

[1] Gajdzik B, Wolniak R, Nagaj R, Žuromskaitė-Nagaj B, Grebski WW. The influence of the global energy crisis on energy efficiency: a comprehensive analysis. Energies. 2024;17:947.

[2] Flottmann J. Australian energy policy decisions in the wake of the 2022 energy crisis. Econ Anal Policy. 2024;81:238-248.

[3] Li RJ, Niu WJ, Zhao WW, Yu BX, Cai CY, Xu LY, *et al*. Achievements and challenges in surfactants-assisted synthesis of MOFs-derived transition metal–nitrogen–carbon as highly efficient electrocatalysts for ORR, OER, and HER. Small. 2025;21:e2408227.

[4] Yu M, Li A, Kan E, Zhan C. Substantial impact of spin state evolution in OER/ORR catalyzed by Fe–N–C. ACS Catal. 2024;14:6816-6826.

[5] Yan HM, Wang G, Lv XM, Cao H, Qin GQ, Wang YG. Revealing the potential-dependent rate-determining step of oxygen reduction reaction on single-atom catalysts. J Am Chem Soc. 2025;147:3724-3730.

[6] Jones TE, Teschner D, Piccinin S. Toward realistic models of the electrocatalytic oxygen evolution reaction. Chem Rev. 2024;124:9136-9223.

[7] Reier T, Oezaslan M, Strasser P. Electrocatalytic oxygen evolution reaction on Ru, Ir, and Pt catalysts: a comparative study of nanoparticles and bulk materials. ACS Catal. 2012;2:1765-1772.

[8] Singh SP, Singh P. Effect of temperature and light on the growth of algae species: a review. Renew Sustain Energy Rev. 2015;50:431-444.

[9] McCook L, Jompa J, Diaz-Pulido G. Competition between corals and algae on coral reefs: a review of evidence and mechanisms. Coral Reefs. 2014;19:400-417.

[10] Nguyen LN, Aditya L, Vu HP, Johir AH, Bennar L, Ralph P, *et al*. Nutrient removal by algae-based wastewater treatment. Curr Pollut Rep. 2022;8:369-383.

[11] Stevenson J, Graham L. Ecological assessments with algae: a review and synthesis. J Phycol. 2014;50:437-461.

[12] Anabtawi HM, Lee WH, Al-Anazi A, Mohamed MM, Aly Hassan A. Advancements in biological strategies for controlling harmful algal blooms (HABs). Water. 2024;16:224.

[13] Ren X, Mao M, Feng M, Peng T, Long X, Yang F. Fate, abundance and ecological risks of microcystins in aquatic environments: implications of microplastics. Water Res. 2024;251:121121.

[14] Abdel-Wareth AAA, Williams AN, Salahuddin M, Gadekar S, Lohakare J. Algae as an alternative source of protein in poultry diets for sustainable production and disease resistance. Front Vet Sci. 2024;11:1382163.

[15] Ahmed N, Sheikh MA, Ubaid M, Chauhan P, Kumar K, Choudhary S. Marine algae diversity, bioactive compounds, health benefits, regulatory issues, and food and drug applications. Measurement: Food. 2024;14.

[16] Chen Y, Zhang Y, Meng H, Cui J, Hayat W, Zhuo Y, *et al*. Insight into algae-derived boron-doped biochar for efficient peroxydisulfate activation. J Environ Chem Eng. 2025;13.

[17] Rafee V, Razaghizadeh A, Nakhaei R, Hosini R. Eco-friendly dye-sensitized solar cells: green synthesis of ZnO nanoparticles using *Sargassum* algae. Mater Sci Eng B. 2025;317:118164.

[18] Patnaik R, Bagchi SK, Rawat I, Bux F. Nanotechnology for the enhancement of algal cultivation and bioprocessing. Bioresour Technol. 2024;406:131025.

[19] Prabhahar M, Prakash S, Dharsan P, Elumalai PV, Xueyi F, Hasan N. Optimization of thermal barrier coating with copper oxide nanoparticles in CI engine using algae methyl ester as fuel. Sci Rep. 2025;15:21221.

[20] Muhyuddin M, Filippi J, Zoia L, Bonizzoni S, Lorenzi R, Berretti E, *et al*. Waste face surgical mask transformation into crude oil and nanostructured electrocatalysts. ChemSusChem. 2022;15:e202102351.

[21] Kaur P, Verma G, Sekhon SSS. Biomass-derived hierarchical porous carbon materials as oxygen reduction reaction electrocatalysts. Prog Mater Sci. 2019;102:1-71.

[22] Sekar S, Sim DH, Lee S. Electrocatalytic hydrogen evolution performance of partially graphitized activated carbon nanobundles derived from human hair waste. Nanomaterials (Basel). 2022;12:531.

[23] Chen W, Gong M, Li K, Xia M, Chen Z, Xiao H, *et al*. Insight into KOH activation mechanism during biomass pyrolysis. Appl Energy. 2020;278:115730.

[24] Zhang C, Chen WH, Saravanakumar A, Lin KYA, Zhang Y. Comparison of torrefaction and hydrothermal carbonization of high-moisture microalgal feedstock. Renew Energy. 2024;225:120265.

[25] Sakaguchi R, Ghosh A, Sawada Y, Takahama K, Nishida Y, Honda M. Thermal isomerization of astaxanthin esters in *Haematococcus lacustris*. Food Biosci. 2024;61:104645.

[26] Pastrana-Pastrana ÁJ, Rodríguez-Herrera R, Solanilla-Duque JF, Flores-Gallegos AC. Plant proteins, insects, edible mushrooms and algae as sustainable protein alternatives. J Future Foods. 2025;5:248-256.

[27] Lu J, Wang B, Qiao Y, Ogino K, Si H, Li Y. Structure and slow-release performance of seaweed biochar. ACS Sustain Chem Eng. 2025;13:9164-9176.

[28] Dong R, Tang Z, Chen Y, Wang X, Cheng W, Hu Q, *et al*. Catalytic pyrolysis of microalgae using nitrogen-rich algae-based modified biochar. Energy. 2025;331:137028.

[29] da Silva AF, Moreira AF, Miguel SP, Coutinho P. Recent advances in microalgae encapsulation techniques for biomedical applications. Adv Colloid Interface Sci. 2024;333:103297.

[30] Chen Z, Yun S, Wu L, Zhang J, Shi X, Wei W, *et al*. Waste-derived catalysts for water electrolysis: circular economy-driven sustainable green hydrogen energy. Nanomicro Lett. 2022;15:4.

[31] Ramanathan S, Lau WJ, Goh PS, Gopinath SCB, Rawindran H, Omar MF, *et al*. Tailoring molecularly imprinted polymer on titanium–multiwalled carbon nanotube functionalized gold electrode for enhanced chlorophyll determination in microalgae health assessment. Mikrochim Acta. 2024;191:586.

[32] Song D, Han X, Li J, Cheng W, Liu C, Wu C, *et al*. Migration of membrane fouling with minimal damage to cell integrity by catalytic ceramic membrane systems under low ozone dosage during algae-laden water treatment. Chem Eng J. 2024;500:156636.

[33] Bhanu M, Mohit A, Remya N. Polyculture microalgae and ZnO/GAC nanocomposite system for greywater treatment. Biomass Bioenergy. 2024;190:107391.

[34] Santos JRD, Raimundo RA, Oliveira JFGdA, Hortencio JS, Loureiro FJA, Macedo DA, *et al*. Eco-friendly high-entropy oxide rock-salt structures for oxygen evolution reaction obtained by green synthesis. J Electroanal Chem. 2024;961:118191.

[35] Zhang R, Sun J, Chen Y, Shen Q, Ding C, Zhang S, *et al*. Advanced porous platinum-group metal nanostructured electrocatalysts for water electrolysis, fuel cells and metal–air batteries. Coord Chem Rev. 2025;543:216958.

[36] Li L, Tang X, Wu B, Huang B, Yuan K, Chen Y. Advanced architectures of air electrodes in zinc–air batteries and hydrogen fuel cells. Adv Mater. 2024;36:e2308326.

[37] Antolini E. Application of 2D graphitic carbon nitride and hexagonal boron nitride in low-temperature fuel cells. Molecules. 2025;30:1852.

[38] Quílez-Bermejo J, Daouli A, Dalí SG, Cui Y, Zitolo A, Castro-Gutiérrez J, *et al*. Electron transfer from encapsulated Fe_3C to the outermost N-doped carbon layer for superior oxygen reduction reaction. Adv Funct Mater. 2024;34:2403810.

[39] Zhang J, Li S, Lu H, Zhu L, Wu F. Lighting strategy drives ammonia nitrogen and phosphate removal in microalgae–bacteria consortia under tetracycline exposure. Algal Res. 2025;88:103989.

[40] Ali SS, Al-Tohamy R, Al-Zahrani M, Schagerl M, Kornaros M, Sun J. Advancements and challenges in microalgal protein production as a sustainable alternative protein source. Microb Cell Fact. 2025;24:61.

[41] Wang C, Wei W, Wu L, Liu X, Duan H, Chen Z, *et al*. Electron donor-driven microalgae upgrading into high-value fatty acids via a microbial platform. ACS ES&T Eng. 2024;4:3080-3091.

[42] Valasara V, Ahn B, Liu JJ, Yu BY, Han SM, Won W. Coproduction of drop-in biofuels and biodegradable plastic monomers: process design and integrative analyses. ACS Sustain Chem Eng. 2025;13:6992-7004.

[43] Ma L, Hu X, Min Y, Zhang X, Liu W, Lam PKS, *et al*. Microalgae-derived single-atom oxygen reduction catalysts for zinc–air batteries. Carbon. 2023;203:827-834.

[44] Shen Y, Liu P, Li Y, Wu J, Song Y, Guo J. In situ observation of defect evolution of graphene nanoflakes in Pt/C catalysts for enhanced ORR performance. Carbon. 2024;230:119669.

[45] Wang K, Yang J, Liu W, Yang H, Yi W, Sun Y, *et al*. Self nitrogen-doped carbon derived from microalgae via lipid extraction pretreatment for oxygen reduction reaction. Sci Total Environ. 2022;821:153155.

[46] Devault DA, Pierre R, Marfaing H, Dolique F, Lopez PJ. Sargassum contamination and consequences for downstream uses: a review. J Appl Phycol. 2020;33:567-602.

[47] He B, Zheng X, Wang K, Liang W, Jia L, Sun J, *et al*. Mild and efficient pretreatment strategy for high-value utilization of cellulose derived from *Sargassum* spp. Int J Biol Macromol. 2025;306:141339.

[48] González RV, Velasco Gómez MY, Mendoza JS, Verde Gómez JY, Guerrero LC. Enhanced extraction of calcium alginate and 2D nanocellulose from brown algae (*Sargassum* spp.). Mater Lett. 2025;398:138941.

[49] Zeferino González I, Valenzuela-Muñiz AM, Verde Gómez Y. Atomic rearrangement of carbon and silicon derived from *Sargassum* spp. and its effect on oxygen reduction reaction activity. Int J Hydrogen Energy. 2025;141:1109-1117.

[50] Yang Y, Li H, Hu Z, Guo J, Li X, Liu P, *et al*. Oxygen control of large-diameter N-type monocrystalline silicon under large thermal fields. Silicon. 2023;16:753-763.

[51] Zeferino González I, Valenzuela-Muñiz AM, Verde-Gómez Y. Si–CN catalysts for oxygen reduction reaction in alkaline media: effect of synthesis temperature. Int J Hydrogen Energy. 2022;47:30187-30195.

[52] Fu X, Wang QD, Liu Z, Peng F. Si-doped carbon nanotubes as efficient metal-free electrocatalysts for oxygen reduction in alkaline medium. Mater Lett. 2015;158:32-35.

[53] Huang H, Wei X, Gao S. Nitrogen-doped porous carbon derived from *Malachium aquaticum* biomass as an efficient oxygen reduction electrocatalyst. Electrochim Acta. 2016;220:427-435.

[54] Tang PD, Du QS, Li DP, Dai J, Li YM, Du FL, *et al*. Fabrication and characterization of graphene microcrystals from lignin refined from sugarcane bagasse. Nanomaterials (Basel). 2018;8:565.

[55] Wang F, Li Q, Xiao Z, Jiang B, Ren J, Jin Z, *et al*. Conversion of rice husk biomass into electrocatalysts for oxygen reduction reaction in Zn–air batteries. J Colloid Interface Sci. 2022;606:1014-1023.

[56] Escobar B, Pérez-Salcedo KY, Alonso-Lemus IL, Pacheco D, Barbosa R. N-doped porous carbon from *Sargassum* spp. as metal-free oxygen reduction electrocatalysts. Int J Hydrogen Energy. 2017;42:30274-30283.

[57] Moreno-Anguiano O, Alvarado-Flores JJ, Rutiaga-Quiñones JG, Márquez-Montesino F, Rojas-López M, Rangel-Méndez JR, *et al*. Feasibility and properties of activated carbons obtained from *Sargassum* spp. Algal Res. 2025;91:104219.

[58] Wang Y, Li S, Qi J, Li H, Han K, Zhao J. Preparation and characterization of super-activated carbon from coupled coal/*Sargassum* precursors. Chin J Chem Eng. 2025;77:81-92.

[59] Pereira L, Cotas J, Gonçalves A. Seaweed proteins: a step toward sustainability? Nutrients. 2024;16:1123.

[60] Inicka A, Lukaszewicz JP. Marine and freshwater feedstocks as precursors for nitrogen-containing carbons: a review. Mar Drugs. 2018;16:142.

[61] Wang D, Hu J, Wei J, Liu X, Hou H. Role of graphitic and pyridinic nitrogen in nitrogen-doped carbon for oxygen reduction reaction. ChemPhysChem. 2023;24:e202200734.

[62] Zhang J, Xia M, Wang J, Wu C, Li S, Liu L, *et al*. High-content graphitic-N self-doped porous carbon derived from seaweed for efficient oxygen reduction reaction. Ionics. 2025;31:4643-4660.

[63] Chen W, Yang H, Chen Y, Xia M, Chen X, Chen H. Transformation of nitrogen and evolution of nitrogen-containing species during algae pyrolysis. Environ Sci Technol. 2017;51:6570-6579.

[64] Fernandez-Escamilla HN, Guerrero-Sanchez J, Contreras E, Ruiz-Marizcal JM, Alonso-Nunez G, Contreras OE, *et al*. Atomistic understanding of oxygen reduction reaction selectivity on nitrogen-doped graphitic carbon. Adv Energy Mater. 2020;11:2002459.

[65] Zeng L, Li X, Fan S, Mu J, Qin M, Wang X, *et al*. Seaweed-derived nitrogen-rich porous carbon as bifunctional materials for oxygen reduction and toluene adsorption. ACS Sustain Chem Eng. 2019;7:5057-5064.

[66] Dong Y, Niu M, Liang JY, Dong L, Xie J, Yang C. Honeycomb-like porous carbon frameworks for stable SiO_x/C anodes. ACS Appl Mater Interfaces. 2025;17:45660-45667.

[67] Faisal SN, Haque E, Noorbehesht N, Zhang W, Harris AT, Church TL, *et al*. Pyridinic and graphitic nitrogen-rich graphene for high-performance supercapacitors and metal-free bifunctional electrocatalysts for ORR and OER. RSC Adv. 2017;7:17950-17958.

[68] Zhang Y, Song X, Huang R, Ye Y, Cheng F, Li H. Sustainable route from kelp to porous MnO/C network anode for high-capacity lithium-ion batteries. J Mater Sci. 2020;55:10740-10750.

[69] Chen Z, Han N, Wei W, Chu D, Ni BJ. Dual doping: an emerging strategy to construct efficient metal catalysts for water electrolysis. EcoEnergy. 2024;2:114-140.

[70] Zi Y, Zhang C, Zhao J, Cheng Y, Yuan J, Hu J. Structure evolution and durability modulation of Ir- and Ru-based OER catalysts under acidic conditions. Small. 2024;20:e2406657.

[71] Wang YZ, Yang M, Ding YM, Li NW, Yu L. Recent advances in complex hollow electrocatalysts for water splitting. Adv Funct Mater. 2021;32:2108681.

[72] Ma N, Jia Y, Yang X, She X, Zhang L, Peng Z, *et al*. Seaweed biomass-derived (Ni,Co)/CNT nanoaerogels as efficient bifunctional electrocatalysts for oxygen evolution and reduction reactions. J Mater Chem A. 2016;4:6376-6384.

[73] Li P, Cheng Z, Chai W, Yao Y, Zhang N, Yue H, *et al*. Anchored Ru clusters on lignin/algae carbon aerogels as efficient bifunctional catalysts for water splitting. New J Chem. 2024;48:9856-9861.

[74] Jeon OS, Hong DP, La Y, Lee JH, Choi MS, Park SY, *et al*. Entangled sodium alginate quasi-solid electrolyte with enhanced air pockets for low-temperature Zn–air batteries. Adv Energy Mater. 2025;15:2500796.

[75] Qiao D, Li H, Shi W, Lu J, Zhang L, Zhang B, *et al*. Effect of agar content on sol–gel behavior and mechanical properties of starch/agar binary systems. Carbohydr Polym. 2022;278:118906.

[76] Santos JRD, Raimundo RA, Silva TR, Silva VD, Macedo DA, Loureiro FJA, *et al*. Mixed-valence oxide nanoparticles synthesized using agar-agar from red algae for oxygen evolution reaction. Nanomaterials (Basel). 2022;12:3170.

[77] Wei X, Song S, Cai W, Kang Y, Fang Q, Ling L, *et al*. Pt nanoparticle–Mn single-atom pairs for enhanced oxygen reduction reaction. ACS Nano. 2024;18:4308-4319.

[78] Ferreira LS, Silva TR, Santos JRD, Silva VD, Raimundo RA, Morales MA, *et al*. Structure, magnetic behavior and OER activity of $CoFe_2O_4$ powders synthesized using agar-agar from red seaweed. Mater Chem Phys. 2019;237:121847.

[79] Wang R, Zhang H, Fang Q, Su ZM, Qiu S. Covalent organic framework-based catalysts for electrosynthesis of hydrogen peroxide: recent advances. Chem Commun. 2025;61:4308-4319.

[80] Akshita, Gupta TK, Gupta D, Chandel NK, Mishra M. Contribution of women in green chemistry: catalyst for a sustainable tomorrow. Sustain Chem Pharm. 2024;42:101823.

[81] Long Y, Chen Z, Wu L, Liu X, Hou YN, Vernuccio S, *et al*. Electrocatalytic CO_2 reduction to alcohols: progress and perspectives. Small Sci. 2024;4:2400129.

[82] Wang G, Chen Z, Xie J, Ding L, Zhu J, Wei W, *et al*. Electrochemical nitrate reduction to ammonia: recent trends and prospects with emphasis on cobalt catalysts. Coord Chem Rev. 2025;539:216751.

[83] Chen Z, Wei W, Shon HK, Ni BJ. Designing bifunctional catalysts for urea electrolysis: progress and perspectives. Green Chem. 2024;26:631-654.

[84] Pal M, Yesankar PJ, Dwivedi A, Qureshi A. Biotic control of harmful algal blooms: a brief review. J Environ Manage. 2020;268:110687.

[85] Hou C, Chu ML, Guzman JA. Risk assessment of harmful algal bloom occurrence in agroecosystems using hydro-ecologic modeling. Ecol Indic. 2022;145:109617.

[86] Tan K, Sun Y, Zhang H, Zheng H. Effects of harmful algal blooms on physiology, immunity and stress resistance of bivalves. Aquaculture. 2023;563:739000.

[87] Wang H, Man S, Wang H, Presser V, Yan Q. Repurposing harmful algal biomass as carbon-based catalysts for nitrogen fertilizer electrosynthesis. Chem Eng J. 2024;497:154455.

[88] Hu X, Liu WJ, Ma LL, Yu HQ. Sustainable conversion of harmful algae biomass into CO_2 reduction electrocatalysts. Environ Sci Technol. 2023;57:1157-1166.

[89] Wu Q, Guo L, Wang Y, Zhao Y, Jin C, Gao M, *et al*. Phosphorus uptake, distribution and transformation by *Chlorella vulgaris* under different trophic modes. Chemosphere. 2021;285:131366.

[90] Huang Y, Lou C, Luo L, Wang XC. Nitrogen and phosphorus coupling effects on mixotrophic *Chlorella vulgaris* growth. Sci Total Environ. 2021;752:141747.

[91] Kusvuran S. *Chlorella vulgaris* alleviates drought stress in broccoli by improving nutrient uptake and antioxidative defense. Hortic Plant J. 2021;7:221-231.

[92] Mei Z, Liu W, Zhou W, Li L, Chen S, Xie S, *et al*. Electrolytic conversion of CO_2 to tunable syngas using Ni–N doped carbon derived from *Chlorella* sp. Electrochim Acta. 2024;508:145271.

[93] Kumar SA, Narasimman K. Utilization of algal biomass-derived carbon in alkaline water electrolysis for hydrogen production. Renew Energy. 2025;254:123760.

[94] Ruban AM, Singh G, Bahadur R, Sathish CI, Vinu A. Almond skin-derived porous biocarbon nanoarchitectonics for CO_2 adsorption and supercapacitors. Carbon. 2024;228:119372.

[95] Neethu B, Ihjas K, Chakraborty I, Ghangrekar MM. Nickel-adsorbed algae biochar as oxygen reduction reaction catalyst. Bioelectrochemistry. 2024;159:108747.

[96] Salo T, Salovius-Laurén S. Green algae as bioindicators for long-term nutrient pollution along coastal gradients. Ecol Indic. 2022;140:109034.

[97] Mohseni A, Fan L, Roddick FAR. Impact of microalgae species and salinity on treatment of wastewater reverse osmosis concentrate. Chemosphere. 2021;285:131487.

[98] Li M, Li Y, Zhang Y, Xu Q, Iqbal MS, Xi Y, *et al*. Role of phosphorus in algal growth and subsequent ecological responses. J Freshw Ecol. 2022;37:57-69.

[99] Xu K, Zou X, Xue Y, Qu Y, Li Y. Seasonal temperature and photoperiod effects on municipal wastewater treatment by algae–bacteria systems. Algal Res. 2021;54:102175.

[100] Lan J, Liu P, Hu X, Zhu S. Harmful algal blooms in eutrophic marine environments: causes, monitoring and treatment. Water. 2024;16.

[101] Sun H, Wang Y, He Y, Liu B, Mou H, Chen F, *et al*. Microalgae-derived pigments for the food industry. Mar Drugs. 2023;21:82.

[102] Li J, Xiong Z, Zeng K, Zhong D, Zhang X, Chen W, *et al*. Nitrogen characteristics and evolution in heavy components of algae pyrolysis bio-oil. Environ Sci Technol. 2021;55:6373-6385.

[103] Yue W, Yu Z, Zhang X, Liu H, Chen Z, Chen J, *et al*. Multi-heteroatom self-doped carbon materials prepared via one-step carbonization for supercapacitors and CO_2 adsorption. Sep Purif Technol. 2025;373:133609.